Acidosis promotes the metastatic colonization of lung cancer via remodeling of the extracellular matrix and vasculogenic mimicry

WAN-YI SHIE[1], PIN-HSUAN CHU[1], MARK YEN-PING KUO[2,3], HUEI-WEN CHEN[4], MENG-TIE LIN[1], XUAN-JIE SU[1], YI-LING HONG[1] and HAN-YI ELIZABETH CHOU[1,3,5]

[1]Graduate Institute of Oral Biology; [2]Department of Dentistry, College of Medicine, National Taiwan University; [3]Department of Dentistry, National Taiwan University Hospital; [4]Graduate Institute of Toxicology, College of Medicine, National Taiwan University, Taipei 100; [5]Center for Biotechnology, National Taiwan University, Taipei 106, Taiwan, R.O.C.

Received November 23, 2022; Accepted July 12, 2023

DOI: 10.3892/ijo.2023.5584

Abstract. Acidosis is a hallmark of the tumor microenvironment caused by the metabolic switch from glucose oxidative phosphorylation to glycolysis. It has been associated with tumor growth and progression; however, the precise mechanism governing how acidosis promotes metastatic dissemination has yet to be elucidated. In the present study, a long-term acidosis model was established using patient-derived lung cancer cells, to identify critical components of metastatic colonization via transcriptome profiling combined with both *in vitro* and *in vivo* functional assays, and association analysis using clinical samples. Xenograft inoculates of 1 or 10 acidotic cells mimicking circulating tumor cell clusters were shown to exhibit increased tumor incidence compared with their physiological pH counterparts. Transcriptomics revealed that profound remodeling of the extracellular matrix (ECM) occurred in the acidotic cells, including upregulation of the integrin subunit α-4 (*ITGA4*) gene. In clinical lung cancer, *ITGA4* expression was found to be upregulated in primary tumors with metastatic capability, and this trait was retained in the corresponding secondary tumors. Expression of ITGA4 was markedly upregulated around the vasculogenic mimicry structures of the acidotic tumors, while acidotic cells exhibited a higher ability of vasculogenic mimicry *in vitro*. Acidosis was also found to induce the enrichment of side population cells, suggesting an enhanced resistance to noxious attacks of the tumor microenvironment. Taken together, these results demonstrated that acidosis actively contributed to tumor metastatic colonization, and novel mechanistic insights into the therapeutic management and prognosis of lung cancer were discussed.

Correspondence to: Dr Han-Yi Elizabeth Chou, Graduate Institute of Oral Biology, National Taiwan University, 1 Changde Street, Taipei 100, Taiwan, R.O.C.
E-mail: hyechou@ntu.edu.tw

Abbreviations: ECM, extracellular matrix, CTCs, circulating tumor cells; *ITGA4*, integrin subunit α-4; GO, Gene Ontology; PPI, protein-protein interaction; KEGG, Kyoto Encyclopedia of Genes and Genomes; PAS, periodic acid-Schiff; BP, biological process; CC, cellular component; MF, molecular function

Key words: acidosis, metastasis, colonization, ECM, vasculogenic mimicry

Introduction

As tumor cells opt for the 'Warburg effect' phenotype to fuel cellular expansion via aerobic glycolysis (1), lactic acid and CO_2 are subsequently produced with a concomitant accumulation of H^+, culminating in a measurable drop in the tumor extracellular pH (2). This increase in acidity of the tumor microenvironment, also termed acidosis, has been described in several cancer types, including lung cancer (3), breast cancer (4,5), head and neck cancer (6), cervical cancer (7) and sarcoma (8), and has been demonstrated to be associated with advanced tumor aggressiveness (9,10). Notably, in a study comparing clinical samples from various cancer types, metastatic lung tumors were demonstrated to display the highest degree of acidosis, with a 7.2-fold increase in lactate concentration compared with non-metastatic lung tumor specimen (11), while metastatic head and neck tumors exhibit the second largest increase in lactate concentration (a 2.6-fold increase) (6). Several studies have also associated differing degrees of acidosis with cellular changes in metabolism, stemness properties and immune evasion ability (12-17), suggesting that acidosis may actively participate in cancer progression. Furthermore, blocking proton transport has been linked to improved clinical outcomes in breast cancer, suggesting that acidosis may also serve as a putative druggable target in therapeutic interventions (18-20). However, despite the supporting evidence that has been collected in this regard, whether acidosis serves an active role in cancer, or is merely a consequence of altered tumor metabolism, remains to be confirmed experimentally.

For metastasis to successfully occur, tumor cells need to overcome multiple challenges prior to the final establishment as a new tumor colony. Once primary tumor cells have overcome the physical constraints set by the surrounding

tissues to gain access into the vascular systems, these cells are confronted with harsh threats, including immune surveillance and the tangential shear force exerted by the blood flow on the surface of the circulating tumor cells (CTCs) (21-23). After extravasation, rapid acquisition of nutrients is required to support the growth of the new colony. The variety of these challenges highlights that tumor cells need to acquire multiple characteristics to survive as a metastatic colony in the new environment. Several animal models have been successfully employed to address different aspects of metastasis, including spontaneous metastasis, heterotopic transplantation and genetic engineering metastasis models (24). Although these models have provided important insights over time, one potential disadvantage is that they may highlight certain specific components of the metastatic process, while underrepresenting changes involved in other steps of metastasis. For instance, the knowledge of critical events involved in the mechanism through which founder CTCs establish a new colony, with its subsequent development, remains poor due to the lack of a suitable study model.

In a set of experiments using the dorsal window chamber model, Estrella *et al* (25) observed that acidic pH in the tumor environment promotes local invasion of breast cancer. Nevertheless, to the best of our knowledge, the mechanism(s) via which acidosis participates in metastatic colonization after extravasation and contributes to secondary tumor establishment remain largely unknown. Therefore, the present study used a novel metastatic colonization model, clinical samples and complementary *in vitro* assays to elucidate the role of long-term acidosis in lung cancer metastasis.

Materials and methods

Cell lines and long-term acidosis. Human CLS1 cells were isolated from an 87-year-old male patient with lung adenosquamous carcinoma who provided written informed consent, according to the protocol NTUH-IRB201103028RC approved by National Taiwan University Hospital Research Ethics Committee (Taipei, Taiwan) (26). These cells were cultured in RPMI-1640 medium supplemented with 10% FBS and 1 mM sodium pyruvate (all from Thermo Fisher Scientific, Inc.) at 37˚C with 5% CO_2 in a humidified incubator. For the establishment of pH 6.6 and pH 7.4 subclones by long-term acidosis treatment, cells were cultured in media adjusted to pH 6.6 as described previously (27) for 2 months, while the control pH 7.4 subclone cells were cultured in pH 7.4 media. Mother stocks of the acidotic and control cells were prepared upon reaching the 48th passage. All experiments were performed using cells at passage 50. In experiments assessing short-term acid treatment, the cells were cultured in the corresponding pH media for 24 h.

Time-lapse microscopy. pH 7.4 or pH 6.6 cells were seeded in 6-well plates at a density of 2,000 cells/well, and live images were captured every 40 min over a period of 96 h using an inverted phase-contrast light microscopy equipped with the ASTEC-real time cell monitoring system (Astec Co., Ltd.). Cell doubling times were analyzed by visual inspection of the serial images and calculated as the time between two completed cytokinesis events.

Trypan blue exclusion assay. pH 7.4 or pH 6.6 cells (20,000 cells/well) were seeded in 6-well plates as triplicates, and cultured for 0, 24, 48, 72 or 96 h at 37˚C before harvesting. Cells were stained with trypan blue (Thermo Fisher Scientific, Inc.) for 30 sec at room temperature to exclude non-viable cells, and counted using a Bright-Line™ hemocytometer (Reichert, Inc.) under a DMi1 inverted light microscope (Leica Camera AG).

MTT assay. To analyze the cellular mitochondrial metabolic rate, pH 7.4 or pH 6.6 cells (1,000 cells/well) were seeded in 96-well plates and cultured for 24, 48, 72 or 96 h at 37˚C, before incubation with 20 μl 5 mg/ml MTT (Merck KGaA) diluted in 180 μl complete medium (RPMI-1640 medium with 10% FBS and 1 mM sodium pyruvate) for 2 h. MTT was subsequently removed, and 100 μl/well DMSO (Bionovas Biotechnology Co., Ltd.) was added and cells were incubated for 15 min. Optical absorbance was measured at 570 nm using an Elx800 reader (BioTek Instruments, Inc.).

Metastatic colonization model. All animal protocols were reviewed and approved by the National Taiwan University College of Medicine Institutional Animal Care and Use Committee (approval no. 20170550; Taipei, Taiwan). A total of 60 female nude mice (BALB/cAnN.Cg-*Foxn1*^{nu}/CrlNarl mice; age, 4 weeks; mean weight, 14.71±1.21 g) were purchased from National Applied Research Laboratories, National Laboratory Animal Center (Taipei, Taiwan), and kept at 22±2˚C and 55±10% humidity with a 12/12-h light/dark cycle, with free access to food and water. In experiment #1, 8 mice were implanted subcutaneously with 10-cell inoculates of pH 6.6 or pH 7.4 cells to simulate metastatic colonization at opposite flanks, while the same procedure was performed with 1-cell inoculates in another 8 mice. In experiment #2, 18 nude mice were implanted subcutaneously with 10 pH 6.6 or pH 7.4 cells at opposite lower flanks, while 1 pH 6.6 or pH 7.4 cell was implanted at opposite upper flanks of the same recipient mouse. In experiment #3, the same procedure as in experiment #2 was performed using 26 nude mice. Briefly, pH 6.6 or pH 7.4 cells at passage 50 were resuspended in complete culture medium, before accurately selecting either 10 or 1 cells under a Zeiss Axio Observer D1 inverted fluorescence microscope (Zeiss AG) and packing these together by natural gravity in 5 μl Growth Factor Reduced, Phenol Red-Free Matrigel™ (Corning, Inc.; final concentration, 50%) for subcutaneous injection into the 5-week-old nude mice using 4% isoflurane for induction and 2% isoflurane for maintenance of anesthesia. Body weight was recorded every other day starting from the time when a palpable tumor could be detected (18 to 20 days post-implantation; Fig. S1). Tumor volume was measured every other day using a caliper and calculated as 1/2 (length x width^2), where length refers to the longest dimension and width refers to the smallest dimension perpendicular to the length. Intolerable distress caused to the animals, such as continued declining weight loss ≥20% for up to 2 days, or a xenograft tumor volume reaching 2,000 mm^3, were set as the humane endpoints of the present study. Mice were euthanized at week 6 post-implantation in a CO_2 chamber for 5 min (CO_2 flow set to 30% chamber volume displacement per min). The mice were observed for

an additional 5 min to determine death as judged by stopped breathing, heart arrest and loss of blink reflex. Dissection was performed to thoroughly inspect any subcutaneous tumors that may have developed. The tumors were extracted, and their volumes were recorded. No further metastasis was observed. The tumor burden observed was: maximum tumor diameter, 9.44 mm; maximum sum of diameter, 16.84 mm; and maximum tumor volume, 308.225 mm^3. The samples were fixed in 4% paraformaldehyde at room temperature for 24 h, followed by histological analyses. Notably, mouse no. 18 of experiment 2 was euthanized at day 35 post-tumor inoculation after observation of clinical signs including dullness, lethargy and failure to respond to stimuli as suggested by the ethical guidelines of the National Taiwan University College of Medicine Institutional Animal Care and Use Committee (Taipei, Taiwan).

Transcriptome sequencing and analyses. For long-term acidosis treatment, two independent transcriptome analysis experiments with two biological replicates each were performed for both pH 6.6 and pH 7.4 cells. CLS1 cells treated with either 0-h (short term, pH 7.4) or 24-h acidosis (short term, pH 6.6) served as short-term treatment references. Total RNA was extracted using TRIzol® reagent (cat. no. 26073; Thermo Fisher Scientific, Inc.) and an RNeasy Mini Kit (cat. no. 74106; Qiagen, Inc.). Only samples with an integrity number >9.0 were used to construct the sequencing libraries using the TruSeq Stranded mRNA Library Prep Kit (cat. no. 20020595; Illumina, Inc.). Briefly, mRNA purification was performed using oligo(dT)-coupled magnetic beads. Double-stranded cDNAs were synthesized using the SuperScript™ II Reverse Transcriptase kit (cat. no. 18064-014; Thermo Fisher Scientific, Inc.) and random primers. The reverse transcription temperature protocol was 10 min at 25˚C, 15 min at 42˚C and 15 min at 70˚C, then holding at 4˚C. The quality of the libraries was assessed on the Agilent Bioanalyzer 2100 system and a Real-Time PCR system (Agilent Technologies, Inc.). The loading concentration of the final libraries was 290 pM as measured by the Qubit 2.0 Fluorometer Q32866 (Thermo Fisher Scientific, Inc.). Sequencing was performed using an Illumina™ NovaSeq 6000 System (Illumina, Inc.) with the NovaSeq 6000 S1 Reagent Kit (300 cycles; cat. no. 20012863; Illumina, Inc.) at a depth of ~40 million reads per sample of 150-bp paired-end reads. Bases with low quality and sequences from adapters in raw data were removed using the program FASTQ (version 0.20.0) (28). The filtered reads were mapped with Bowtie 2 (https://bowtie-bio.sourceforge.net/bowtie2/index.shtml) and aligned to the human reference genome hg19 as it provided the most comprehensive annotation available at the time of analysis. The software FeatureCounts v2.0.1 (29) in the Subread package v2.0.1 (https://subread.sourceforge.net/) was applied for quantification of the gene abundance. Differentially expressed genes were identified by DESeq2 version 1.28.0 (30) for the samples with biological replicates or by EdgeR version 3.36.0 (31) for the samples without biological replicates (0 and 24 h acidosis samples). Significant differential expression of genes was defined as a posterior probability of being equally expressed (PPEE) <0.05 and $\log_2$ |posterior fold change|>1. Data were deposited in the National Center for Biotechnology Information Gene Expression Omnibus database (accession no. GSE200546; https://www.ncbi.nlm.nih.gov/geo/query/acc.cgi?acc=GSE200546).

Gene Ontology (GO), Kyoto Encyclopedia of Genes and Genomes (KEGG) and protein-protein interaction (PPI) analyses. Cellular component (CC), molecular function (MF) and biological process (BP) functions were analyzed using the GO database (http://geneontology.org/) using Protein Analysis Through Evolutionary Relationships 15.0 (https://pantherdb.org/) with a significance threshold of P<0.05 and false discovery rate <0.05. KEGG signaling pathway analyses were subsequently performed using KEGG Orthology-Based Annotation System 3.0 (32) for the *Homo sapiens* reference list, with a significance threshold of P<0.05 and corrected P<0.05. PPI analyses were performed using the Search Tool for the Retrieval of Interacting Genes/Proteins (STRING) database version 10.5 (https://string-db.org; >0.5 confidence score; species was limited to *Homo sapiens*).

Histological and immunohistochemistry staining. For H&E staining, xenograft samples were fixed in 4% paraformaldehyde at room temperature for 24 h and then embedded in paraffin. Sections (4-μm thick) were de-paraffinized with xylene (Merck KGaA) for 5 min at room temperature and rehydrated with a gradient of 95, 85, 70 and 50% ethanol for 5 min each at room temperature prior to a 2-min incubation at room temperature with H&E Y solution (ScyTek Laboratories, Inc.). Images of all sections were captured using a Zeiss Axio Imager Z2 upright fluorescence microscope (Zeiss AG).

For immunohistochemistry staining, human lung cancer tissue microarray slides (LC10014a, LC10013c and LC814a; 10% formalin-fixed for 24 h at room temperature, paraffin-embedded; 5-μm thick) were purchased from US Biomax, Inc.; TissueArray.Com LLC as approved by National Taiwan University Hospital Research Ethics Committee (approval no. 202201055RIND; Taipei, Taiwan). Xenograft samples including both paired and unpaired tumors were fixed in 4% paraformaldehyde for 24 h at room temperature, paraffin-embedded and cut as sections of 4-μm thick. All slides were de-paraffinized with xylene (Merck KGaA) for 5 min at room temperature and rehydrated with a gradient of 95, 85 and 70% ethanol for 5 min each at room temperature. Antigen retrieval was performed in 10 mM citric acid buffer at 100˚C for 20 min followed by 3% H_2O_2 treatment for 20 min at room temperature. Blocking using Protein block (normal goat serum reagent as supplied by the manufacturer; cat. no. HK112-9KE; BioGenex) was performed for 30 min at room temperature. The slides were incubated with anti-human ITGA4 antibodies (cat no. 350695; dilution, 1:500; United States Biological) for 2 h at room temperature and then washed with PBS buffer three times. The slides were incubated with HRP rabbit/mouse antibodies (undiluted; cat. no. K5007: Dako; Agilent Technologies, Inc.) for 1 h at room temperature. 3,3-diaminobezidine chromogenic staining was used for detection prior to 5 sec hematoxylin counterstaining at room temperature. LC814a included 6 cases of small cell carcinoma and 17 cases each of squamous cell carcinoma and adenocarcinoma, as well as their matched lymph node metastases. LC10014a included 50 cases of adenocarcinoma, and LC10013c included 48 cases of adenocarcinoma with the

matched adjacent normal lung tissues (NATs) and 4 normal lung tissues. There were 13 overlapping cases among these three lung tissue arrays, which were annotated and analyzed only once to avoid repetition. Images of all sections were captured using a Zeiss Axio Imager Z2 upright fluorescence microscope (Zeiss AG) and analyzed using StrataQuest 6.0.1.216 software (TissueGnostics GmbH) for at least three randomly selected fields.

Vasculogenic mimicry assay. In vitro vasculogenic mimicry assays were performed on 96-well plates coated with 50 μl Growth Factor Reduced, Phenol Red-Free Matrigel™ per well. pH 6.6 and pH 7.4 cells were seeded at a density of $4x10^4$ cells/well and cultured for 10 h. Images of the wells were captured using a Zeiss Axio Observer D1 inverted fluorescence microscope (Zeiss AG). Three independent experiments with three repeats each were performed. Three randomly selected images per sample were analyzed using Image J version 1.53k (National Institutes of Health) for vasculogenic mimicry structures. Five parameters were analyzed: Total tube length, number of branching points, number of loops, percentage of total loop area per well and number of tubes.

To analyze *in vivo* vasculogenic mimicry, paraffin-embedded slides of xenograft samples (4% paraformaldehyde-fixed for 24 h at room temperature; 4-μm thick) were de-paraffinized with xylene (Merck KGaA) for 5 min at room temperature and rehydrated with a gradient of 95, 85 and 70% ethanol for 5 min each at room temperature. The slides were treated with a periodic acid-Schiff PAS-1 staining kit (ScyTek Laboratories, Inc.) according to the manufacturer's instructions. Slides were then processed as for immunohistochemical staining, including antigen retrieval, quenching, blocking, secondary antibody incubation, washing, chromogen detection, and counterstaining as described for immunohistochemical staining. Slides were incubated with polyclonal rabbit anti-human CD31 antibody (cat. no. ab28364; dilution, 1:500; Abcam) for 2 h at room temperature. Images of all sections were captured using a Zeiss Axio Imager Z2 upright fluorescence microscope (Zeiss AG). The angiogenic structures ($CD31^+/PAS^+$) were counted in four biologically paired whole tumors. Vasculogenic mimicry structures were defined by $CD31^-/PAS^+$ staining accompanied by the presence of red blood cells in the lumen, and counted from at least five whole tumors of either pH 6.6 and pH 7.4.

Side population analysis. pH 7.4 or pH 6.6 cells ($1x10^6$ cells/ml) were seeded 14 h before the experiment, then incubated in RPMI-1640 medium containing 2% FBS (both from Thermo Fisher Scientific, Inc.) and 7.5 μg/ml Hoechst 33342, with either DMSO (Mock group) or the ATP-binding cassette (ABC) transporter inhibitor reserpine (20 μM; Reserpine group) (all from Merck KGaA) for 2 h at 37˚C in the dark, then treated with 0.05% Trypsin-EDTA for resuspension in sorting buffer containing 50 μg/ml propidium iodide (both from Thermo Fisher Scientific, Inc.) to exclude non-viable cells. Cells were subsequently sorted by dual wavelength analysis (blue, 424-444 nm; red, 675 nm) with an excitation wavelength of 350 nm using a BD FACS Aria II flow cytometer (Becton, Dickinson and Company). Data were analyzed using FCS Express 4 Plus (De Novo Software), and the fold-change of ABC transporter-dependent side population cells was calculated as [pH 6.6 (side population $\%^{Mock}$-side population $\%^{Reserpine}$)]/[pH 7.4 (side population $\%^{Mock}$-side population $\%^{Reserpine}$)].

Western blot analysis. Cell lysates were collected using a buffer containing 50 mM Tris/HCl (pH 8.0), 1% SDS, 1% deoxycholate and 10 mM EDTA, supplemented with cOmplete™ Protease Inhibitor Cocktail (cat. no. 11836145001; Roche Diagnostics) and phosphatase inhibitor cocktail 3 (cat. no. P0044; Merck KGaA), and the lysates were centrifuged at 4˚C at 12,000 x g for 5 min. The protein concentration was determined using a BCA protein assay kit (Thermo Fisher Scientific, Inc.), and aliquots containing 20 μg total protein per lane were analyzed by 10% SDS-PAGE and blotted onto a PVDF membrane (Pall Corporation). The membranes were blocked with TBS buffer containing 0.05% Tween-20 and 5% skimmed milk for 30 min at room temperature. After a 2-h incubation at room temperature with the primary antibodies, including rabbit anti α-tubulin antibody (cat. no. GTX112141; dilution, 1:1,000; GeneTex, Inc.), rabbit anti-Oct4 antibody (cat. no. SC9081; dilution, 1:500; Santa Cruz Biotechnology, Inc.) and rabbit anti-mouse Nanog antibody (cat. no. RCAB002P; dilution, 1:500; ReproCELL, Inc.). The membranes were washed with TBS buffer containing 0.1% Tween-20 three times at room temperature before incubation with secondary antibodies (goat anti-rabbit HRP antibody; cat. no. GTX213110; dilution, 1:5,000; GeneTex, Inc.), for 1 h at room temperature. Bands were visualized using the ECL chemiluminescence method (WesternBright® ECL HRP substrate; Advansta, Inc.) with an LAS-4000 luminescent image analyzer (FUJIFILM Wako Pure Chemical Corporation).

Statistical analysis. Unless otherwise specified, all experiments were repeated independently at least three times. The mean values of the groups were compared, and the results are presented as the mean ± SD. GraphPad Prism 7 software (Dotmatics) and OriginPro 2023b software (OriginLab) were used for statistical analysis. Comparisons between different groups were analyzed by Student's unpaired t-test. In paired tumors, the germination times, volume, density, the percentage of $ITGA4^+$ cells and $ITGA4^+$ stained areas, as well as the analysis of endothelial angiogenic and vasculogenic mimicry structures, were analyzed by Student's paired t-test. In the lung tissue microarray, the mean intensity of expression per $ITGA4^+$ cells was analyzed for tumor different nodal statuses and stages using one-way ANOVA with Tukey's multiple comparisons test. Two-way mixed ANOVA with the Bonferroni multiple comparisons test was used to analyze the percentage of $ITGA4^+$ cells in the normal group vs. (NAT group vs. lung cancer within the same patient group). Two-way mixed ANOVA with the Bonferroni multiple comparisons test was used to analyze the mean intensity of expression per $ITGA4^+$ cells in the no-metastasis group vs. (metastatic primary tumors group vs. lymph node metastases within the same patients group). $P<0.05$ was considered to indicate a statistically significant difference.

Results

Establishment of the long-term acidosis cell model. Tumor acidosis develops over long periods of time, involving serial regulatory processes in the cancer cell that may lead to the acquisition of a stable phenotype (15). To accurately reflect this scenario, a long-term acidosis cell model was established in the present study (Fig. 1A) using the CLS1 patient-derived primary cells of lung adenosquamous carcinoma reported in our previous study (26). These cells were acclimated for 2 months in culture media at pH 6.6 to emulate the cellular responses to acidosis relative to normal physiological culture conditions (pH 7.4) (33,34). Using time-lapse microscopy, both subclones acclimated at pH 6.6 and pH 7.4 were found to replicate synchronously without detectable abnormalities or differences in morphology (Fig. 1B), nor any significant differences in cell doubling time, population survival or metabolic rates (Fig. 1C-E). Cell lines from other cancer types, such as SAS (Tohoku University, Sendai, Japan) and OECM1 (National Defense Medical Center, Taipei, Taiwan) of oral squamous cell carcinoma origin, also exhibited good adaptation to the of acidotic conditions, displaying discernible changes in population survival rates or growth dynamics (data not shown). These finding suggested that the lung cancer cells became well adapted to the long-term acidosis regime, and subsequent analyses could be conducted with only minimal concern regarding discrepancies of growth dynamics.

Numerous studies have reported that an acidic microenvironment can trigger stemness-like properties in tumor cells (35,36). Although western blotting indicated no significant change in the protein expression levels of either of the stemness-associated transcription factors Oct4 and Nanog (Fig. 1F), the pH 6.6 subclones displayed a 1.85-fold increase in the proportion of reserpine-sensitive side population cells relative to the pH 7.4 subclones (Fig. 1G), suggesting a survival advantage of the pH 6.6 subclone associated with ABC transporter-dependent clearance of noxious agents while growing in adverse environments. Taken together, the present results indicated that lung cancer cells can adapt to long-term acidosis, preserving regular cellular morphology and growth dynamics. Acidosis *per se* may not be sufficient to promote the stemness properties of lung cancer cells; however, with an increased proportion of side population cells, acidotic cancer cells may display a survival advantage in adverse environments. The two CLS1 subclones obtained were referred to as pH 6.6 cells and pH 7.4 cells, and they were subsequently used as the model to study the lung cancer cell response following long-term acidosis.

Acidosis promotes metastatic incidence and growth. Overcoming the adverse environment for growth is a primordial task for CTCs to successfully establish as a new metastatic colony (22). To test whether the survival advantage of acidotic cells may lead to increased metastatic colony incidence, a novel experimental model that tightly controlled the exact number and physical conditions of the inoculated cells was designed, to enable a rigorous comparison of the colonizing ability of the pH 7.4 and pH 6.6 cells. Since CTCs found in the pulmonary veins of patients with non-small cell lung cancer (NSCLC) are mostly clusters of ~10 cells (37), exactly 10 cells or one single cell from the pH 6.6 and pH 7.4 cells were selected under an inverted microscope, then packed together by natural gravity in 5 μl growth factor-reduced Matrigel (Fig. 2A). These cells were implanted subcutaneously in opposite flanks of nude mice, which were sacrificed to inspect the tumor growth either on day 42 post-inoculation or earlier if humane endpoint criteria had been reached. After performing three independent experiments, grown tumor masses were retrieved from 27 mice (Fig. S2), while 33 mice did not develop tumors (Fig. S3). As shown in Fig. 2B, the cumulative tumor incidence of the 10-cell and 1-cell inoculations of the pH 6.6 cells surpassed that of the pH 7.4 cells by 2.22- and 1.25-fold, respectively. When comparing paired tumors grown on the same mouse, the germination time of the pH 6.6 tumors was faster (20±1.5 days vs. 25±9.4 days post-inoculation for the pH 7.4 tumors), and their standard deviation was smaller, indicating a more coordinated pace compared with their pH 7.4 counterparts (Fig. 2C); they also exhibited a larger volume with a slightly higher density (Fig. 2D). Albeit without reaching statistical significance, the tumor incidence rate, germination time, volume and density all displayed consistent differences when comparing pH 6.6 tumors with their pH 7.4 counterparts, collectively supporting a more robust establishment of the pH 6.6 cells as developing colonies. This also indicates that, despite the low number of cells inoculated, the metastatic colonization model was able to provide reliable information on the role of long-term acidosis in promoting tumor germination and growth.

Acidosis results in reorganization of the ECM. The molecular events underlying the metastatic advantage of acidotic cells were subsequently investigated. RNA sequencing analysis was employed to profile the transcriptomes of both the pH 6.6 and pH 7.4 cells (Gene Expression Omnibus series accession no. GSE200546; https://www.ncbi.nlm.nih.gov/geo/query/acc.cgi?acc=GSE200546) (38). A total of 1,735 differentially expressed genes (>2-fold change; PPEE <0.05) were identified in two independent RNA sequencing experiments with two biological replicates each (Fig. S4). Of these genes, 142 showed consistent changes in all replicates (Fig. 3A), of which 44 genes were found to be upregulated and 98 genes were downregulated in pH 6.6 cells. Heatmap analysis of these 142 acidosis-responsive genes highlighted the differential expression of numerous ECM-related genes, including *ITGA4*, *FBN1*, *FBN2*, *COL6A1*, *ITGB4* and *VTN* (Fig. 3B). In Table I, the 20 most upregulated and downregulated genes are listed. Furthermore, functional annotation of these 142 acidosis-responsive genes using KEGG database analysis identified 'ECM-receptor interaction' and 'cell adhesion molecules' as the most significantly overrepresented categories. Correspondingly, in the GO enrichment analysis of these acidosis-responsive genes, the terms 'cell adhesion' and 'regulation of cell communication' in the BP category, 'plasma membrane' and 'extracellular region' in the CC category, and 'extracellular matrix structural constituent' in the MF category were the main terms identified (Fig. 3C). Finally, STRING analysis of the protein-protein networks (>0.5 confidence score) revealed that these 142 acidosis-responsive genes gravitated around processes involving 'ECM organization', 'regulation of localization' and 'cellular response to chemical stimulus' (Fig. 3D). Taken together, these results suggested that a coordinated and largescale reorganization of the ECM occurs upon long-term acidosis of lung cancer cells.

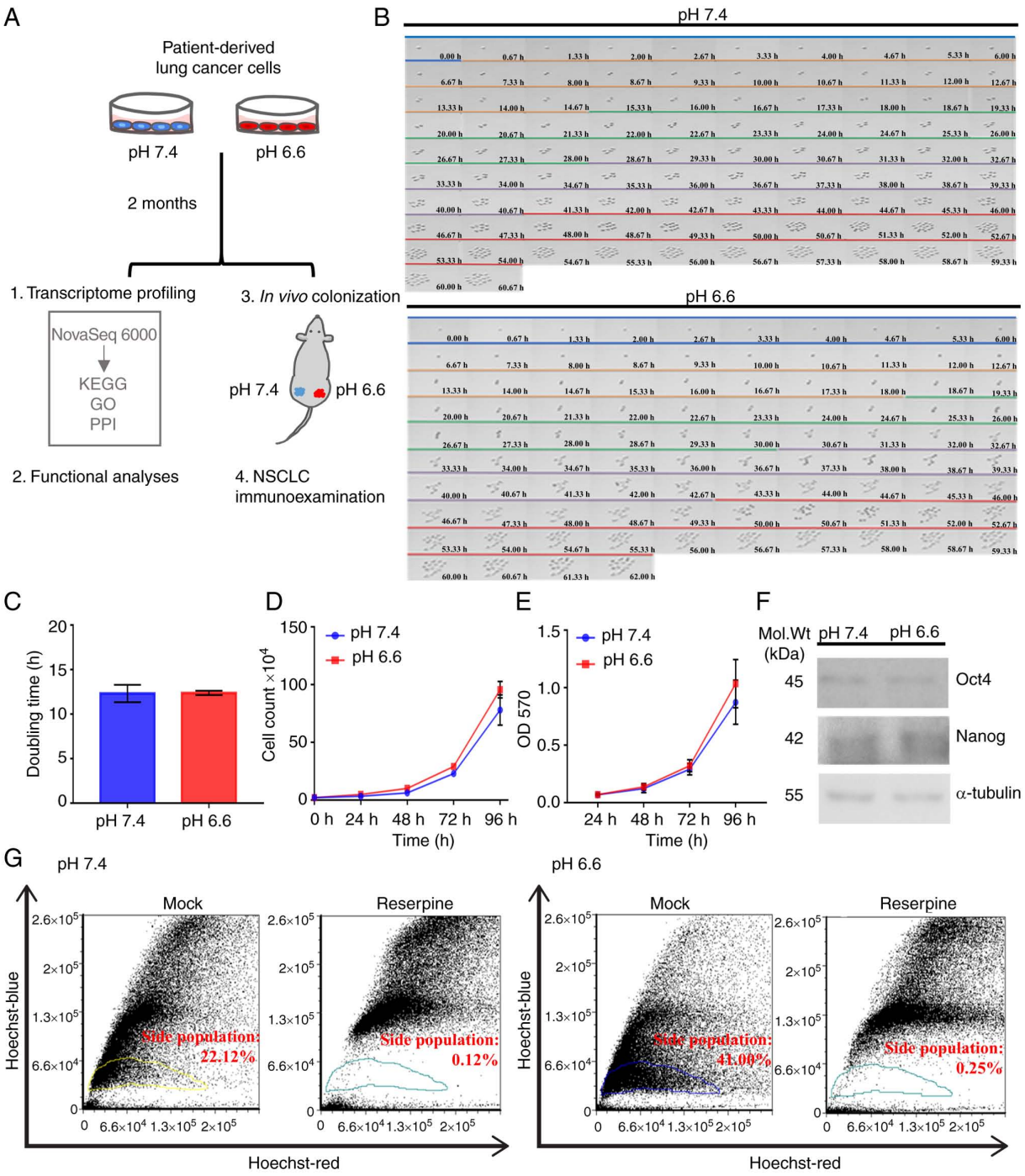

Figure 1. Establishment of long-term acidosis lung cancer cell model. (A) Treatment scheme and analytical approach for long-term acidosis in metastatic colonization. Patient-derived CLS1 lung cancer cells were acclimated for 2 months in pH 7.4 or pH 6.6 media. Both *in vitro* and *in vivo* assays were validated by clinicopathological examination of NSCLC specimens. (B) Time lapse microscopy across 96 h to observe doubling dynamics and morphology at a magnification of x40. Each color bar indicates one doubling generation, from generation 0 (blue) to 4 (red). (C) Average doubling time of cell generations (G0-G4) presented as the mean ± SD from three independent experiments. (D) Viability of pH 7.4 and pH 6.6 cells as examined using trypan blue exclusion assay at 0, 24, 48, 72 and 96 h post-seeding based on three independent experiments. (E) Metabolic curve as determined using MTT assay at 24, 48, 72 and 96 h based on two independent experiments with three replicates each. (F) Protein expression of the stemness-associated transcription factors Oct4 and Nanog. Representative western blot image using 20 μg whole cell lysate per lane. (G) ATP-binding cassette-transporter-dependent clearance activity. Gated areas mark the reserpine-sensitive side population cells. Data were analyzed using Student's unpaired t-test and are presented as the mean ± SD. Mol. Wt, molecular weight; NSCLC, non-small cell lung cancer; OD, optical density; GO, Gene Ontology; PPI, protein-protein interaction; KEGG, Kyoto Encyclopedia of Genes and Genomes.

Increased ITGA4 protein expression in the acidotic metastases. To identify the direct participants of acidosis-induced ECM organization that may offer targetability in terms of future therapeutic interventions, the acidosis-responsive genes annotated to the two GO categories 'extracellular region' and 'plasma membrane', which were also included in the 'ECM organization' category in PPI analysis, were selected. Of the six targets identified, *ITGA4* was found to be the most upregulated gene

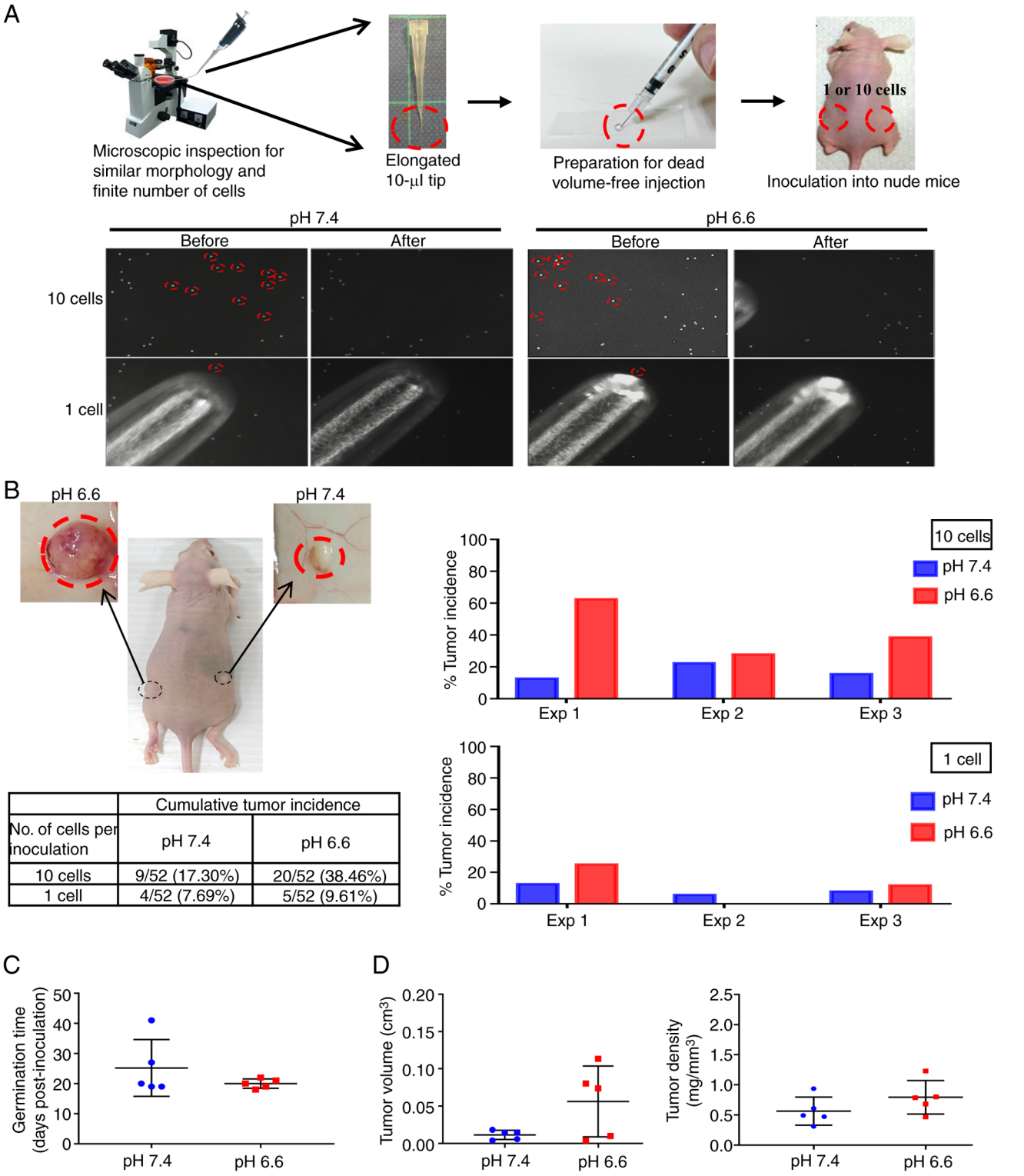

	Cumulative tumor incidence	
No. of cells per inoculation	pH 7.4	pH 6.6
10 cells	9/52 (17.30%)	20/52 (38.46%)
1 cell	4/52 (7.69%)	5/52 (9.61%)

Figure 2. Long-term acidosis promotes the incidence of metastatic colonization. (A) (Top panel) Workflow of the metastatic colonization model. (Lower panel) Picking a finite number of cells using an elongated tip. Each red circle indicates one cell (magnification, x100). (B) Representative image of the xenograft tumors and their cumulative incidence. pH 6.6 and pH 7.4 cells were inoculated at opposite flanks of the same mouse. The circled area indicates the regions where tumors have developed, with their macroscopic appearance recorded post-mortem shown in the upper images. Five mice bearing 10-cell inoculates developed paired tumors grown in the same recipient mouse. Their (C) tumor germination time, and (D) tumor volume and density were analyzed using Student's paired t-test, and are presented as the mean ± SD. Exp, experiment.

as determined by the fold change of the read counts (Fig. 4A). *ITGA4* transcripts were present at low levels in pH 7.4 cells. They encode for the α4 subunit of the integrin protein family, which heterodimerizes with either the β1 or the β7 subunit to form a functional integrin to regulate cell motility and adhesion (39). High and steady levels of *ITGB1* transcripts were found in both the pH 6.6 and 7.4 cell groups, while *ITGB7* was expressed only at negligible levels (Fig. 4B). This suggests that the higher

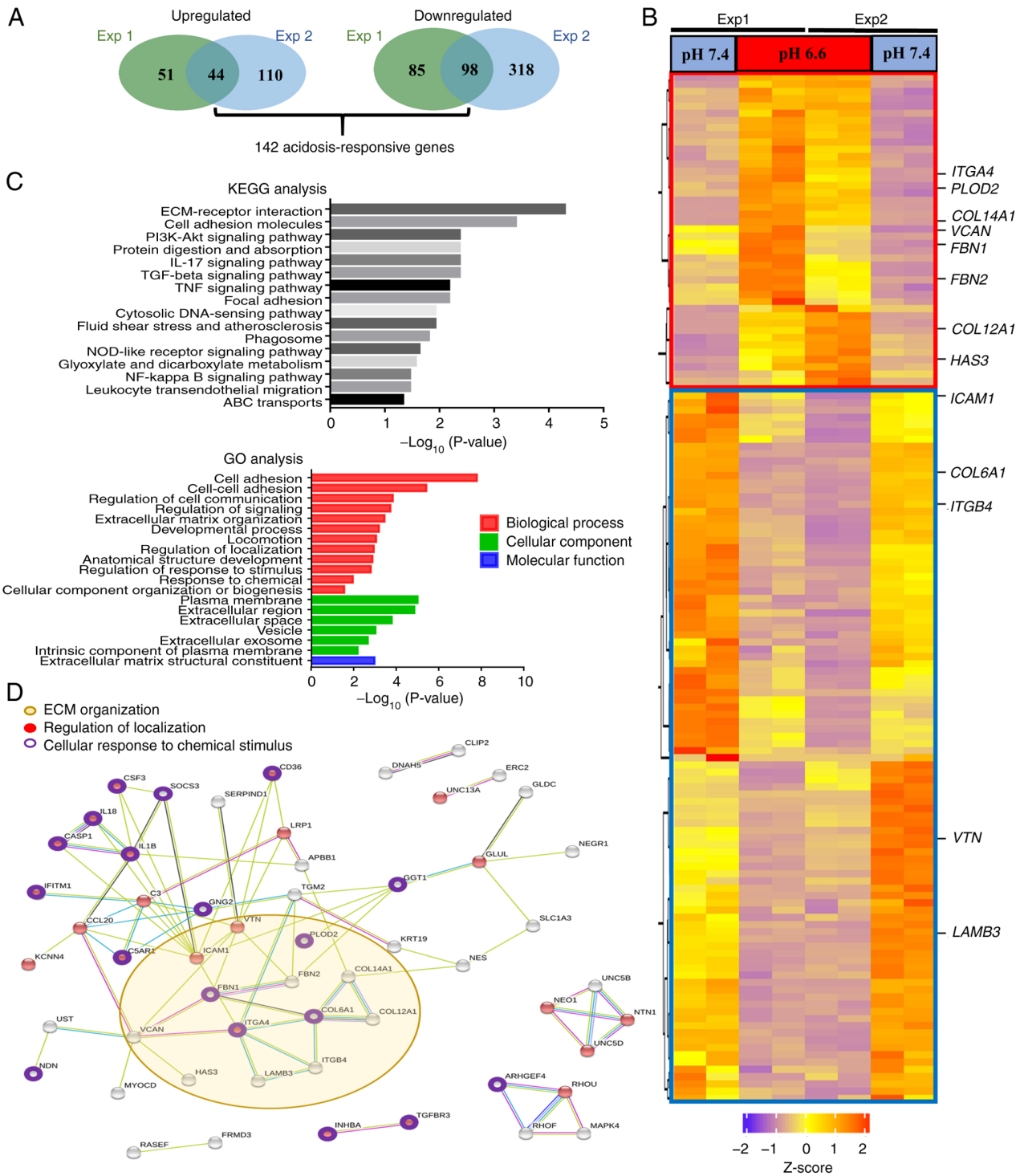

Figure 3. Long-term acidosis induces reorganization of the ECM. (A) A total of 142 acidosis-responsive genes were identified as those showing consistent differential expression with >2-fold change at a posterior probability of being equally expressed <0.05 in two independent RNA sequencing experiments with two repeats each. (B) Heatmap of the 142 acidosis-responsive genes. The red box demarks the 44 upregulated genes, while blue box demarks the 98 downregulated genes in pH 6.6 cells. ECM-associated genes identified by KEGG analysis are indicated. (C) Both KEGG pathway and GO analyses annotated ECM-associated events, including 'ECM-receptor interaction', 'cell adhesion' and 'extracellular matrix structural constituent', as the most prominent changes induced after long-term acidosis. P<0.05 was considered to indicate a statistically significant difference. (D) Protein-protein interaction analysis of the 142 acidosis-responsive genes using the Search Tool for the Retrieval of Interacting Genes/Proteins database. Interactions are color-coded as follows: Blue, gene co-occurrence; black, co-expression; purple, experimentally determined; aqua, curated databases; and olive yellow, text-mining. A confidence score >0.5 was set as the filter value. ABC, ATP-binding cassette; ECM, extracellular matrix; Exp, experiment; GO, Gene Ontology; KEGG, Kyoto Encyclopedia of Genes and Genomes; NOD, nucleotide-binding oligomerization domain.

expression of ITGA4 may result in an increase of functional α4β1 integrin in the pH 6.6 cells. Immunohistochemical examination confirmed that the percentage of ITGA4-expressing cells was significantly higher in the pH 6.6 metastatic tumors, although the increase in the positively stained area was not statistically significant (Fig. 4C). Furthermore, ITGA4 proteins

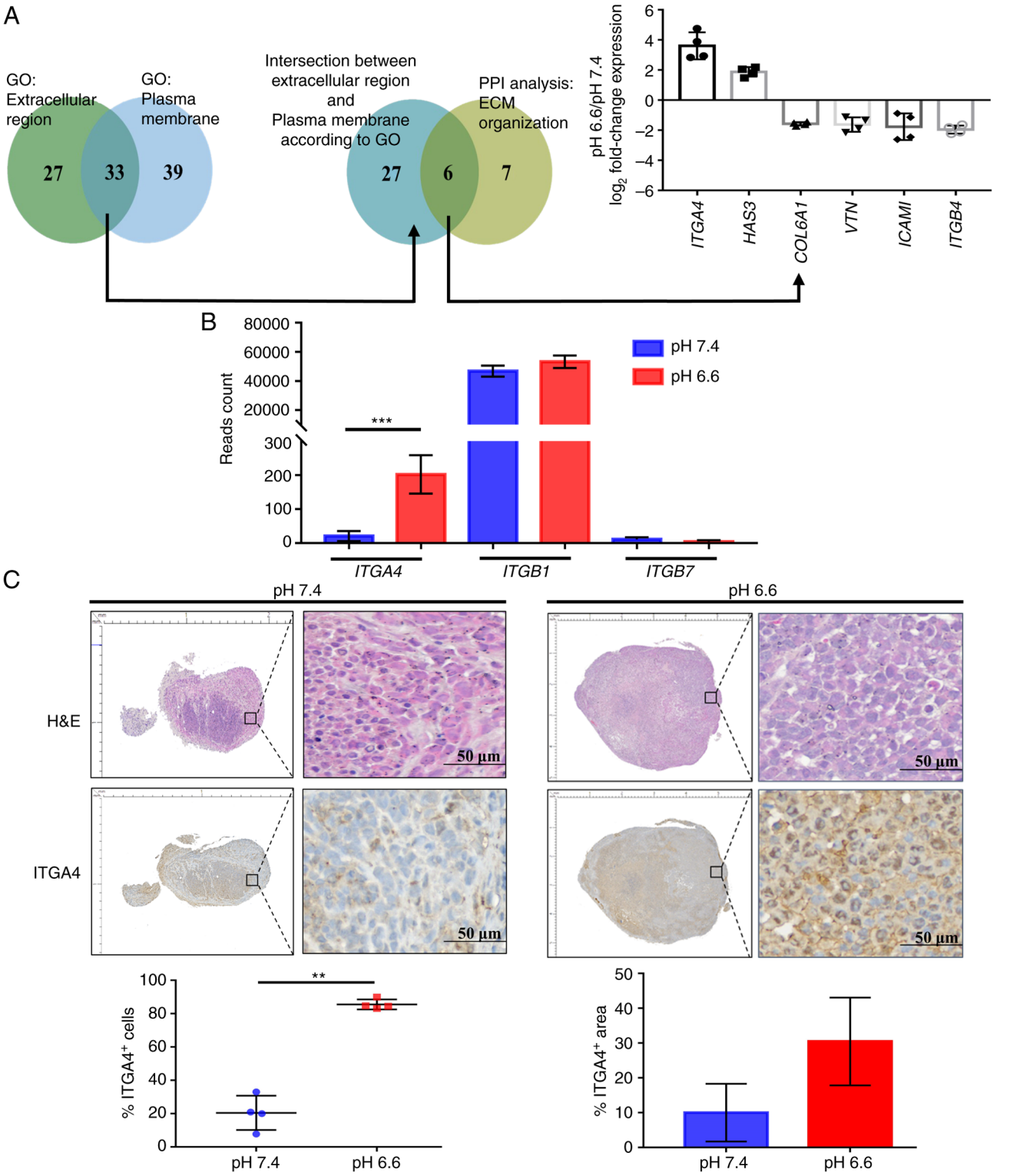

Figure 4. Increased ITGA4 protein expression in the metastatic colonies. (A) Acidosis-responsive genes localized in the outer plasma membrane involved in ECM organization were identified through cross-comparisons among the indicated GO categories and PPI networks. ITGA4 exhibited the highest fold-change in gene expression among these six genes. (B) mRNA levels of the ITGA4 integrin partners extracted from RNA-Seq data were analyzed using Student's unpaired t-test and presented as the mean ± SD. (C) Immunohistochemical staining of ITGA4 protein in the pH 6.6 and pH 7.4 paired metastatic colonies. Percentage of positive cells and positively stained areas as determined by StrataQuest were analyzed using Student's paired t-test and presented as the mean ± SD. Scale bar, 50 μm. **P<0.01 and ***P<0.001 compared with pH 7.4. ECM, extracellular matrix; GO, Gene Ontology; ITGA4, integrin subunit α-4; PPI, protein-protein interaction; RNA-Seq, RNA sequencing.

were demonstrated to be predominantly localized to the cell membrane of the pH 6.6 tumors (Fig. 4C; lower right panel). Taken together, these experiments suggested that acidosis induced the upregulation of *ITGA4* mRNA, which is effectively translated into protein, and this higher level of ITGA4 protein expression was sustained in acidotic metastatic colonies.

Table I. Differentially expressed genes after long-term acidosis.

A, Top 20 upregulated genes

No.	Gene name	Reads FC	log_2FC
1	*TMPRSS15*	2177.5183	11.0885
2	*LEF1*	16.1598	4.0143
3	*COL14A1*	14.8659	3.8939
4	*ITGA4*	13.5348	3.7586
5	*CFI*	12.7163	3.6686
6	*SLITRK6*	10.1096	3.3377
7	*COL12A1*	8.9881	3.1680
8	*ADGRV1*	7.5856	2.9232
9	*NCAM2*	7.2470	2.8574
10	*TENM1*	6.6790	2.7396
11	*NEGR1*	6.3001	2.6554
12	*GNG2*	6.1555	2.6219
13	*MYOCD*	5.2372	2.3888
14	*GPR141*	5.1445	2.3630
15	*RASEF*	4.7859	2.2588
16	*LBH*	4.4340	2.1486
17	*FBN2*	4.2925	2.1018
18	*HAS3*	3.9088	1.9667
19	*GCA*	3.8591	1.9482
20	*OR51B5*	3.8137	1.9312

B, Top 20 downregulated genes

No.	Gene name	Reads FC	log_2FC
1	*SERF1A*	0.0075	-7.0553
2	*CDH11*	0.0378	-4.7272
3	*MAL2*	0.0383	-4.7077
4	*DCLK1*	0.0427	-4.5507
5	*ARHGEF5*	0.0462	-4.4350
6	*ZNF44*	0.0588	-4.0875
7	*NDN*	0.0598	-4.0641
8	*IGSF11*	0.0622	-4.0060
9	*MAPK4*	0.0637	-3.9722
10	*AMDHD1*	0.0696	-3.8445
11	*CSF3*	0.0753	-3.7305
12	*TMEM256-PLSCR3*	0.0869	-3.5250
13	*ERC2*	0.1061	-3.2370
14	*FAM134B*	0.1286	-2.9585
15	*CRIP1*	0.1300	-2.9439
16	*SLCO2B1*	0.1365	-2.8728
17	*AGR2*	0.1404	-2.8321
18	*MYOM3*	0.1409	-2.8270
19	*PLA2R1*	0.1440	-2.7962
20	*CYB5R2*	0.1672	-2.5801

All genes had a posterior probability of being equally expressed value <0.05. FC, fold change.

Long-term acidosis enhances vasculogenic mimicry. In solid tumors, *ITGA4* expression has been implicated in tumor interaction with vascular endothelial cells, which is crucial for proper metastatic colonization and angiogenesis (40,41). To examine the development of vascular structures, all paired tumors that were grown in the same recipient mouse were compared, in order to minimize inter-individual differences in the ability of vascularization. A similar extent of macroscopic neoangiogenic blood vessel formation was observed for pH 6.6 and pH 7.4 tumors (Fig. 5A; left panels). Both tumors were found to be irrigated internally with CD31-positive angiogenic microvessels. By contrast, only the pH 6.6 tumors displayed a large number of $CD31^-/PAS^+$ trabecular structures, indicative of the presence of vasculogenic mimicry in the acidotic tumors, while no such structures were observed in the paired pH 7.4 tumors (Fig. 5A). This observation was sustained even when comparing all grown tumors obtained from the experiment (Fig. S5A), and the accentuated expression of ITGA4 surrounding these structures (Fig. 5B) suggested a possible involvement of ITGA4 in the formation of vasculogenic mimicry. To verify whether long-term acidosis could promote vasculogenic mimicry *in vitro*, live microscopy was employed to compare the potential of vasculogenic mimicry of pH 6.6 cells vs. pH 7.4 cells. The numbers of vasculogenic mimicry loops and branch points formed by pH 6.6 cells were significantly higher, and their total lengths were longer (Fig. 5C). Parameters of potential trabecular space for nutrient infusion, as evaluated by the total loop area per well (Fig. S5B), as well as the quantity of tubes formed (Fig. S5C), were also found to be higher in the acidotic cells. Taken together, these results suggested that long-term acidosis could promote the formation of vasculogenic mimicry networks, thereby enhancing the ability of tumors to establish nutrient and metabolite exchanges in the new colony.

ITGA4 upregulation is not restricted to the cancer cells. Since acidosis may affect the microenvironment beyond the intratumoral milieu, it was subsequently examined whether upregulation of ITGA4 also occurred in the adjacent tissues. Immunohistochemical staining indicated that ITGA4 protein expression in normal lung tissue was low, whereas in normal lung tissues adjacent to the tumors, the presence of ITGA4 was found to be significantly higher, accompanying an even higher expression in the tumor cells themselves (Fig. 6). A 2-fold upregulation of *ITGA4* expression upon challenging the cells with a pH 6.6 environment for 24 h was also observed, suggesting that this increase in the mRNA level was a rapid response to environmental acidosis, which may be further maintained and amplified as acidosis is sustained (Fig. S6). These results indicated that the upregulation of *ITGA4* is a phenomenon common to tissues in the tumor microenvironment, which is further amplified in the tumor cells as acidosis is prolonged.

Upregulation of ITGA4 expression is a signature of primary tumors with metastatic potential. Upregulation of ITGA4 expression has been associated with metastasis in several different tumor types (42-44). To determine the participation of ITGA4 in metastatic colonization, clinical lung cancer specimens were examined, and ITGA4 expression was compared

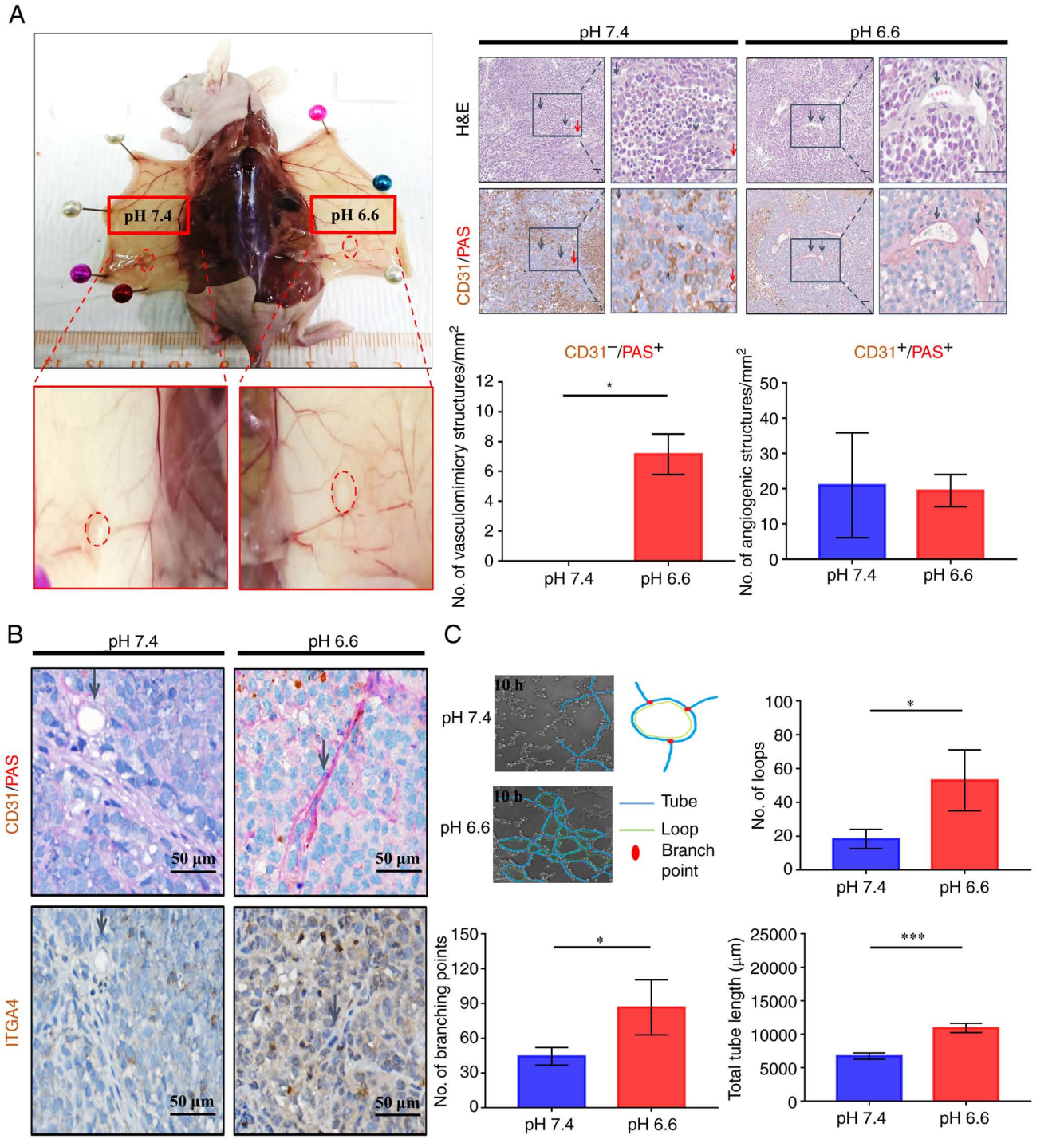

Figure 5. Long-term acidosis promotes vasculogenic mimicry. (A) Vascular structures in the metastatic colonies. Paired tumors grown in the same recipient mouse were compared. Zoomed-in images of the boxed regions are shown (scale bar, 50 μm). Red arrows denote CD31$^+$/PAS$^+$ endothelial angiogenic structures, whereas the blue arrows denote CD31$^-$/PAS$^+$ vasculogenic mimicry structures. Data are presented as the mean ± SD and were analyzed using Student's paired t-test. (B) ITGA4 protein expression adjacent to vasculogenic mimicry structures examined by immunohistochemical staining. Arrows denote CD31$^-$/PAS$^+$ vasculogenic mimicry structures. Scale bar, 50 μm. (C) *In vitro* vasculogenic mimicry capabilities of pH 7.4 and pH 6.6 cells. The number of loops and branching points, and the total tube length were quantified at 10 h post-seeding, and the results are presented as the mean ± SD of three independent experiments and were analyzed using Student's unpaired t-test. *P<0.05 and ***P<0.001 compared with pH 7.4. ITGA4, integrin subunit α-4; PAS, periodic acid-Schiff.

across TNM descriptors. As shown in Fig. 7A, ITGA4 was widely expressed in all adenocarcinoma specimens tested. Notably, compared with the non-metastatic primary tumors, ITGA4 expression as evaluated by mean intensity per positively stained cells was significantly higher in the primary tumors that had already disseminated (N1 and N2+N3; Fig. 7B), whereas the level of ITGA4 expression was not significantly different between the N1 or N2 primary tumors and their corresponding lymph node metastases (Fig. 7C). Similarly, statistical analysis across different stages of lung cancer (Fig. 7D) also indicated that upregulation of ITGA4 expression occurred upon the tumor's entry into stage II (Fig. 7E), whereas neither more

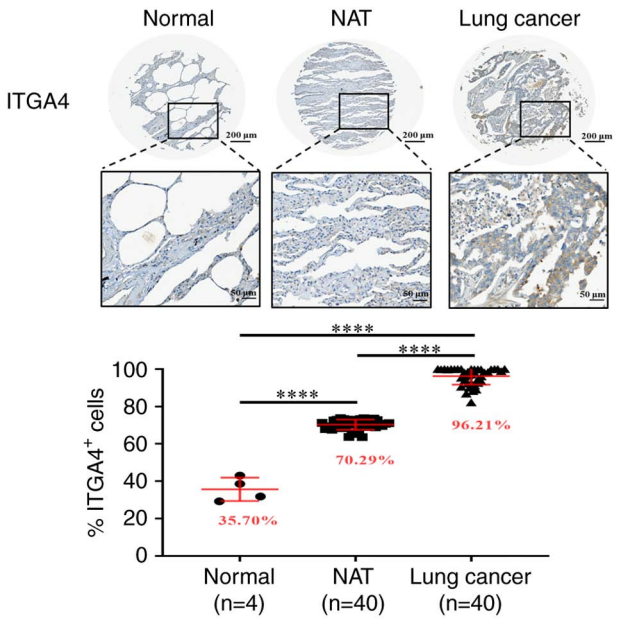

Figure 6. ITGA4 is upregulated in adjacent normal tissues. Representative images of ITGA4 staining in normal lung tissue, NAT and lung cancer. Percentages of ITGA4$^+$ cells are shown. Data are presented as the mean ± SD and were analyzed using a two-way mixed ANOVA with the Bonferroni method for post hoc pairwise comparisons. Magnification, x200. Upper scale bar, 200 μm; lower scale bar, 50 μm. ****P<0.0001 compared with normal or NAT as indicated. NAT, adjacent normal lung tissue; ITGA4, integrin subunit α-4.

advanced stages, nor their corresponding metastases, showed any further significant increase in the ITGA4 level (Fig. 7F). Taken together, these results indicated that the upregulation of ITGA4 is a common feature of primary lung tumors that have developed metastatic potential, and acquisition of a higher level of ITGA4 may be a prerequisite for the successful completion of metastasis to form secondary tumors. Since the upregulation of ITGA4 persists within the lymph node metastases where acidosis may no longer be present, these data also suggested that acidosis may possess the potential to induce long-term regulatory changes that support the continued upregulation of ITGA4 even after extratumoral acidosis pressure is alleviated.

Discussion

An acidic microenvironment presents continuous stress to cells, which respond through adaptation and evolution to achieve dynamic fitness for their survival. As cancer cells are intrinsically prone to genetic changes, long-term acidosis may further promote their pace of evolution, driving the selection for tumor cells with enhanced survival capabilities (45,46). Nevertheless, a systematic analysis of the role of acidosis in cancer progression has been hampered by difficulties, including long experimental time periods, marked individual variabilities and scarcity of *in vivo* probes. Recently, MRI chemical exchange saturation transfer combined with positron emission tomography imaging was used to demonstrate the contribution of acidosis to the metastatic potential of breast cancer cell lines in an animal model (47). In the present study, a metastatic colonization model was established to investigate the effect of long-term acidosis on lung cancer cells. The results indicated that acidosis facilitated the colonization step of metastasis by conferring a growth advantage to the tumor mass, leading to higher tumor incidence rates. Transcriptomics analysis of acidotic cells revealed an extensive reorganization of the ECM, featuring upregulation of the ECM organization gene *ITGA4*. Acidotic tumors exhibited prominent vasculogenic mimicry structures at ITGA4-rich regions, while the acidotic cells also displayed an improved vasculogenic mimicry ability *in vitro*, suggesting a role of the ITGA4 protein in the facilitation of nutrient supply in the growing tumor mass. In summary, the present study provided evidence that acidosis promoted the establishment of CTCs as new metastatic colonies after extravasation via remodeling of the ECM and vasculogenic mimicry (Fig. 8). The present study also demonstrated that upregulation of ITGA4 expression occurred in both tumor and adjacent normal tissues, indicating that acidosis affects not only the tumor, but also induces changes in the surrounding tissues.

In the present experimental animal model, the initial events of metastatic colonization at distant organs were simulated by the subcutaneous implantation of exactly 10 tumor cells or only 1 tumor cell, reflective of the number of CTCs in the pulmonary vein of patients with NSCLC (37). This technique is derived from the tumor incidence stemness assay in our previous study (26), with improvements to tightly control the exact number and physical conditions of the inoculated cells. As the number of cells implanted was low, tumors did not develop in all mice (Fig. S3) (26), and no further metastasis or internal tumors were observed in the experimental time span (42 days post-inoculation). Three individual experiments were conducted using the same procedures, with a gradual increase in the number of animals used each time based on the gained experience. This approach was taken to cope with the expected low incidence of tumor formation and taking ethical considerations into account, while still obtaining robust and reproducible findings. Notably, the inoculation of paired tumors at both flanks of the same mouse allowed comparisons of tumor development free of individual differences, which revealed a growth advantage of the acidotic cells, despite the divergent measurements observed among different experimental animals. No medium/buffer/vector control group was needed in this experimental design as the test group pH 6.6 cells were compared with the control group pH 7.4 cells. We hypothesized that this novel animal model can emulate the scenario of metastatic colonization, thus offering a study model that complements other metastasis tumor models currently in use, including spontaneous metastasis (48), tail vein injection (49) and genetically engineered mouse models (50).

Our previous study reported the strong positive association between the ECM component fibronectin and the metastatic potential of lung cancer cells (51). Fibronectin is an integrin α4β1 ligand (52), and the present study also revealed that the fibronectin-interacting genes *FBN1* and *FBN2* (53) were upregulated in acidotic cells. Furthermore, the whole transcriptome dataset suggested that the change of ECM composition is an extensive and coordinated event, involving other extracellular components, such as collagen type XIV α-1 chain and collagen type XII α1 chain. The individual contribution of these genes in terms of acidosis-induced ECM remodeling and vasculogenic mimicry requires further investigation. Our preliminary

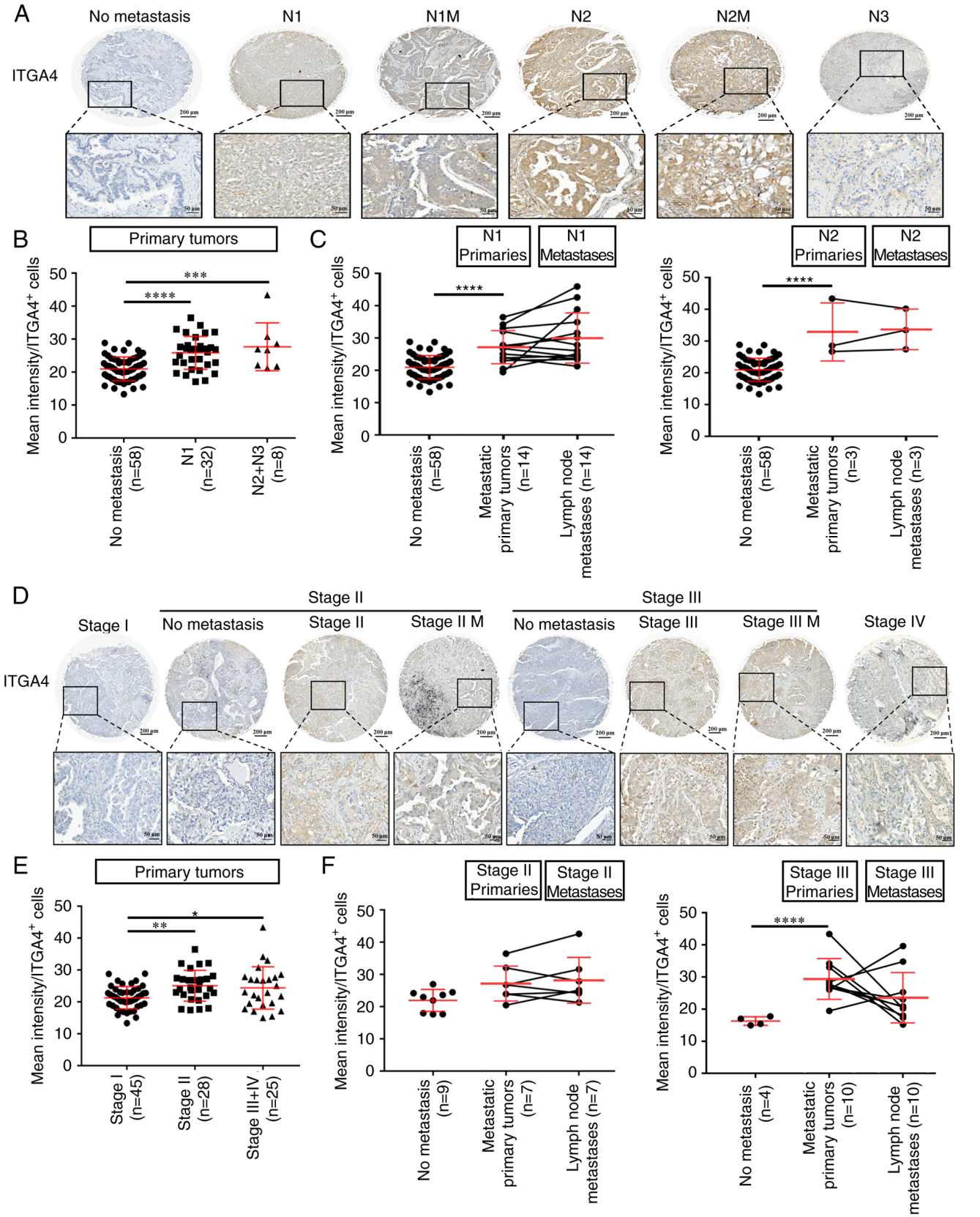

Figure 7. Upregulation of ITGA4 expression is a signature of primary tumors with metastatic potential. (A) Representative images of ITGA4 expression in lung cancer for different nodal statuses. (B) ITGA4 expression was calculated as the mean intensity of staining per ITGA4-positive cells, and analyzed by one-way ANOVA with Tukey's multiple comparisons test. (C) ITGA4 expression at the primary site of N1 or N2 tumors compared with their corresponding lymph node metastases, as analyzed by two-way mixed ANOVA with the Bonferroni method for post hoc pairwise comparisons. (D) Representative images of ITGA4 expression in lung cancer at different stages. (E) ITGA4 expression in primary tumors at different cancer stages as analyzed by one-way ANOVA with Tukey's multiple comparisons test. (F) ITGA4 expression at the primary site of stage II or III tumors compared with their corresponding lymph node metastases, as analyzed by two-way mixed ANOVA with the Bonferroni method for post hoc pairwise comparisons. Magnification, x200. Upper scale bar, 200 μm; lower scale bar, 50 μm. *P<0.05, **P<0.01, ***P<0.001 and ****P<0.0001. ITGA4, integrin subunit α-4; M, matched lymph node metastatic site of the same tumor; N, nodal status.

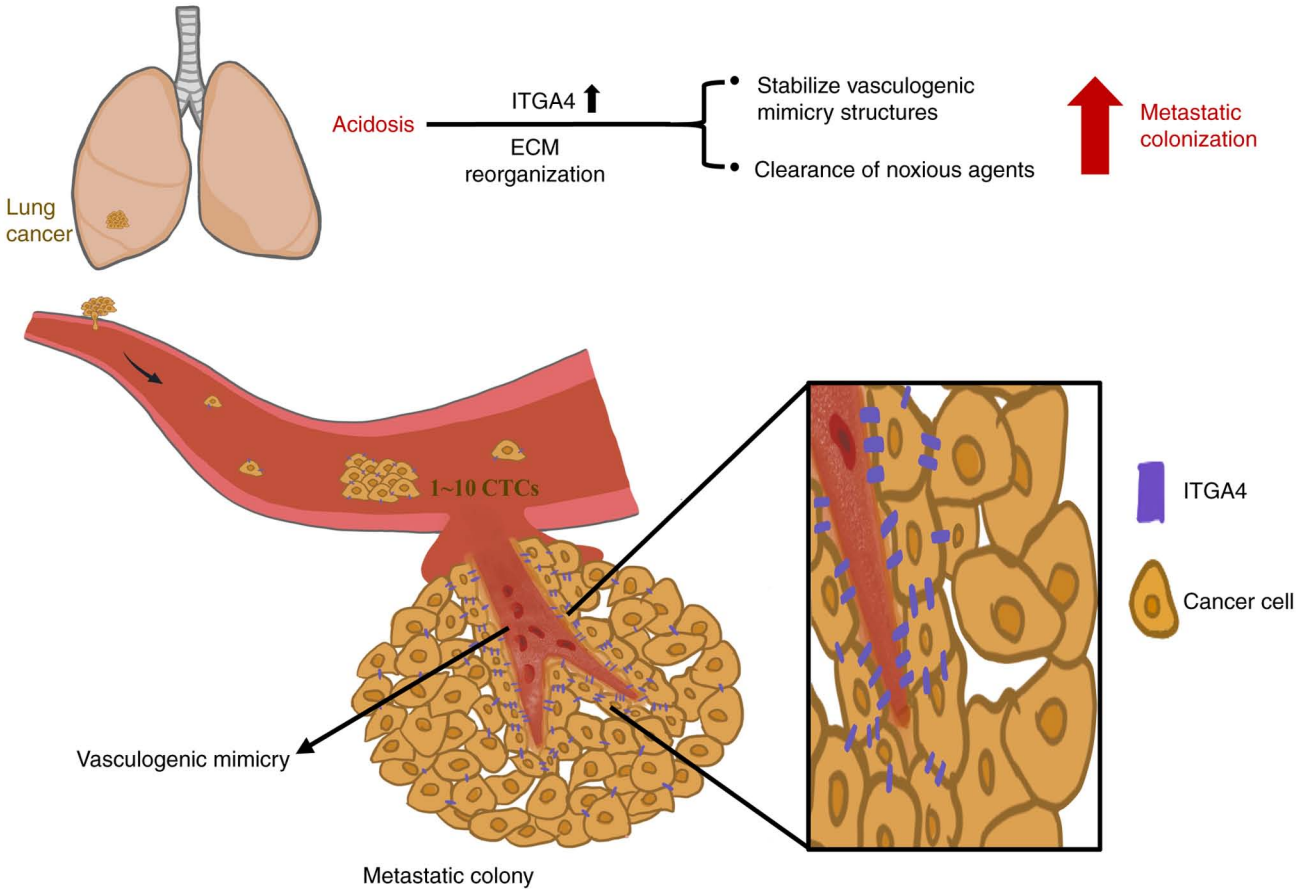

Figure 8. Acidosis contributes to metastatic colonization via remodeling of the ECM and vasculogenic mimicry. Long-term acidosis reprograms the transcriptome profile of lung cancer cells, characterized by extensive changes in the ECM composition. Upregulation of ITGA4 expression is associated with the stabilization of vasculogenic mimicry structures and clearance of noxious metabolites, thus promoting the establishment of CTCs as new metastatic colonies after extravasation. CTCs, circulating tumor cells; ECM, extracellular matrix; ITGA4, integrin subunit α-4.

results regarding ectopic overexpression of full-length ITGA4 cDNA have revealed that the sole manipulation of *ITGA4* gene expression was not sufficient to recapitulate the complete phenotype elicited by long-term acidosis (data not shown). Perturbations of cell adhesion and proliferation also made it difficult to evaluate the effects of altering ITGA4 levels compared with the mock transfection control. Similarly, in melanoma cells (54), it has been reported that overexpression of ITGA4 induces homotypic adhesion of the cells in the form of integrin α4β1 interaction. These observations also highlight the pleiotropic and longitudinal nature of long-term acidosis, and that its final effects on cancer progression are an integrated outcome involving multiple players/steps over time, which cannot be recapitulated by the transient manipulation of ITGA4 expression alone.

ITGA4 encodes for a member of the integrin α family (39), which forms a heterodimeric transmembrane protein with either the β1 or the β7 subunit to function in cell adhesion and expansion. The present study revealed that both the mRNA and protein expression levels of ITGA4 were increased in long-term acidotic cells, with accentuated localization of ITGA4 around the vascular mimicry structures of the tumors. It has been reported that upregulation of ITGA4 is associated with poor prognosis of numerous types of tumors (42-44,55). ITGA4 has also been implicated in the activation of the Hedgehog signaling pathway, enhancing cancer cell stemness and tumorigenicity, and stabilizing cell clusters (56). The present study corroborates the findings of these studies, by demonstrating the increase in tumor incidence, chemoresistance properties and vasculogenic mimicry after long-tern acidosis, which favors the establishment of secondary tumors.

Integrin α4β1 and the hyaluronan ligand CD44 have been reported to synergize in enhancing ABC transporter functionality, thereby promoting tumor chemoresistance (57) and providing protection against noxious agents through limiting their entry into cells (58). The pH 6.6 cells exhibited an ~2-fold increase in the proportion of the side population cells, indicating the involvement of ABC transporter activity. However, our transcriptome analysis indicated no transcriptional upregulation of any of the ABC transporter family genes (data not shown), suggesting that this side population functionality may involve post-transcriptional regulation, as has been reported in human hematopoietic progenitor cells, in which the integrin α4β1/CD44 axis controls side population/drug efflux functionality (57). Although an increase in the proportion of side population cells is a hallmark for the stemness properties of cancer cells (59), the expression levels of the stemness-associated transcription factors Nanog and Oct4 were not found to be increased in the pH 6.6 cells. Taken together, these results suggested that acidotic cells possess a superior ability to

achieve clearance of noxious agents via the ABC transporters, thus promoting the survival of metastatic colonies in the new environment. However, acidosis *per se* may be insufficient to promote the expression of stemness-associated transcription factors Nanog and Oct4 in cancer cells.

The benefits of vasculogenic mimicry in rapidly establishing nutrient supply for the development of metastasis have been described in numerous tumor types, including melanoma (60), head and neck cancer (61), lung cancer (62-64) and colorectal cancer (65). The finding that ITGA4 expression was elevated in the proximity of vasculogenic mimicry structures of the acidosis colonies was in accordance with previous studies demonstrating that integrins are associated with the formation of vasculogenic mimicry (66,67). The present study demonstrated that acidosis enhanced the formation of vasculogenic mimicry networks, which together with the capability to expel noxious agents through ABC transporter activity, could support the survival and expansion of the metastatic colony in new environments. These results suggest a role for acidosis as an intricate factor of cancer progression and shed light on the key molecular role of ITGA4, which may aid the development of therapeutic interventions with the aim of deterring lung tumor metastasis.

Acknowledgements

Not applicable.

Funding

The present study was supported by the grants MOST 107-2314-B-002-197-MY3, MOST106-2314-B-002-140, MOST103-2221-E-002-107-MY3 and MOST 102-2321-B-002-024 from the Ministry of Science and Technology, Taiwan.

Availability of data and materials

The transcriptome analysis datasets generated and/or analyzed during the current study are available in the GEO repository, https://www.ncbi.nlm.nih.gov/geo/query/acc.cgi?acc=GSE200546. All other datasets used and/or analyzed during the current study are available from the corresponding author on reasonable request.

Authors' contributions

WYS contributed to conceptualization of the study, experimentation, methodology, software, visualization, data acquisition, analysis, curation and writing (original draft preparation). PHC performed the experiments. MYPK contributed to the conceptualization of the study and provided resources. HWC contributed to the conceptualization of the study, provided resources and obtained funding. MTL, XJS and YLH performed data curation, data acquisition and analysis. HYEC contributed to project administration, conceptualization of the study, methodology, funding acquisition, writing, reviewing and editing of the manuscript, and supervision. WYS and HYEC confirmed the authenticity of all the raw data. All authors have read and approved the final manuscript.

Ethics approval and consent to participate

All animal protocols were reviewed and approved by the National Taiwan University College of Medicine Institutional Animal Care and Use Committee (approval no. 20170550; Taipei, Taiwan). Usage of human lung cancer tissue microarray slides (LC10014a, LC10013c and LC814a) was approved by National Taiwan University Hospital Research Ethics Committee (approval no. 202201055RIND; Taipei, Taiwan). Human CLS1 cells were isolated from an 87-year-old male patient after the patient provided written informed consent, which was approved by the National Taiwan University Hospital Research Ethics Committee (approval no. NTUH IRB201103028RC; Taipei, Taiwan).

Patient consent for publication

Not applicable.

Competing interests

The authors declare that they have no competing interests.

References

1. Pascale RM, Calvisi DF, Simile MM, Feo CF and Feo F: The Warburg effect 97 years after its discovery. Cancers (Basel) 12: 2819, 2020.
2. Pillai SR, Damaghi M, Marunaka Y, Spugnini EP, Fais S and Gillies RJ: Causes, consequences, and therapy of tumors acidosis. Cancer Metastasis Rev 38: 205-222, 2019.
3. Faubert B, Li KY, Cai L, Hensley CT, Kim J, Zacharias LG, Yang C, Do QN, Doucette S, Burguete D, *et al*: Lactate metabolism in human lung tumors. Cell 171: 358-371.e9, 2017.
4. Kennedy KM, Scarbrough PM, Ribeiro A, Richardson R, Yuan H, Sonveaux P, Landon CD, Chi JT, Pizzo S, Schroeder T and Dewhirst MW: Catabolism of exogenous lactate reveals it as a legitimate metabolic substrate in breast cancer. PLoS One 8: e75154, 2013.
5. Damaghi M, West J, Robertson-Tessi M, Xu L, Ferrall-Fairbanks MC, Stewart PA, Persi E, Fridley BL, Altrock PM, Gatenby RA, *et al*: The harsh microenvironment in early breast cancer selects for a Warburg phenotype. Proc Natl Acad Sci USA 118: e2011342118, 2021.
6. Brizel DM, Schroeder T, Scher RL, Walenta S, Clough RW, Dewhirst MW and Mueller-Klieser W: Elevated tumor lactate concentrations predict for an increased risk of metastases in head-and-neck cancer. Int J Radiat Oncol Biol Phys 51: 349-353, 2001.
7. Walenta S, Wetterling M, Lehrke M, Schwickert G, Sundfør K, Rofstad EK and Mueller-Klieser W: High lactate levels predict likelihood of metastases, tumor recurrence, and restricted patient survival in human cervical cancers. Cancer Res 60: 916-921, 2000.
8. Lora-Michiels M, Yu D, Sanders L, Poulson JM, Azuma C, Case B, Vujaskovic Z, Thrall DE, Charles HC and Dewhirst MW: Extracellular pH and P-31 magnetic resonance spectroscopic variables are related to outcome in canine soft tissue sarcomas treated with thermoradiotherapy. Clin Cancer Res 12: 5733-5740, 2006.
9. Meyer KA, Kammerling EM, *et al*: pH studies of malignant tissues in human beings. Cancer Res 8: 513-518, 1948.
10. Persi E, Duran-Frigola M, Damaghi M, Roush WR, Aloy P, Cleveland JL, Gillies RJ and Ruppin E: Systems analysis of intracellular pH vulnerabilities for cancer therapy. Nat Commun 9: 2997, 2018.
11. Vlachostergios PJ, Oikonomou KG, Gibilaro E and Apergis G: Elevated lactic acid is a negative prognostic factor in metastatic lung cancer. Cancer Biomark 15: 725-734, 2015.
12. Schoonjans CA, Joudiou N, Brusa D, Corbet C, Feron O and Gallez B: Acidosis-induced metabolic reprogramming in tumor cells enhances the anti-proliferative activity of the PDK inhibitor dichloroacetate. Cancer Lett 470: 18-28, 2020.

13. Ning WR, Jiang D, Liu XC, Huang YF, Peng ZP, Jiang ZZ, Kang T, Zhuang SM, Wu Y and Zheng L: Carbonic anhydrase XII mediates the survival and prometastatic functions of macrophages in human hepatocellular carcinoma. J Clin Invest 132: e153110, 2022.
14. Desquiret-Dumas V, Leman G, Wetterwald C, Chupin S, Lebert A, Khiati S, Le Mao M, Geffroy G, Kane MS, Chevrollier A, *et al*: Warburg-like effect is a hallmark of complex I assembly defects. Biochim Biophys Acta Mol Basis Dis 1865: 2475-2489, 2019.
15. Boedtkjer E and Pedersen SF: The acidic tumor microenvironment as a driver of cancer. Annu Rev Physiol 82: 103-126, 2020.
16. Moellering RE, Black KC, Krishnamurty C, Baggett BK, Stafford P, Rain M, Gatenby RA and Gillies RJ: Acid treatment of melanoma cells selects for invasive phenotypes. Clin Exp Metastasis 25: 411-425, 2008.
17. Damaghi M, Tafreshi NK, Lloyd MC, Sprung R, Estrella V, Wojtkowiak JW, Morse DL, Koomen JM, Bui MM, Gatenby RA and Gillies RJ: Chronic acidosis in the tumour microenvironment selects for overexpression of LAMP2 in the plasma membrane. Nat Commun 6: 8752, 2015.
18. Ibrahim-Hashim A and Estrella V: Acidosis and cancer: From mechanism to neutralization. Cancer Metastasis Rev 38: 149-155, 2019.
19. Harguindey S, Alfarouk K, Polo Orozco J, Fais S and Devesa J: Towards an integral therapeutic protocol for breast cancer based upon the new H^+-centered anticancer paradigm of the late post-Warburg era. Int J Mol Sci 21: 7475, 2020.
20. de la Cruz-López KG, Castro-Muñoz LJ, Reyes-Hernández DO, García-Carrancá A and Manzo-Merino J: Lactate in the regulation of tumor microenvironment and therapeutic approaches. Front Oncol 9: 1143, 2019.
21. Massagué J and Obenauf AC: Metastatic colonization by circulating tumour cells. Nature 529: 298-306, 2016.
22. Amintas S, Bedel A, Moreau-Gaudry F, Boutin J, Buscail L, Merlio JP, Vendrely V, Dabernat S and Buscail E: Circulating tumor cell clusters: United we stand divided we fall. Int J Mol Sci 21: 2653, 2020.
23. Chrabaszcz K, Jasztal A, Smęda M, Zieliński B, Blat A, Diem M, Chlopicki S, Malek K and Marzec KM: Label-free FTIR spectroscopy detects and visualizes the early stage of pulmonary micrometastasis seeded from breast carcinoma. Biochim Biophys Acta Mol Basis Dis 1864: 3574-3584, 2018.
24. Gómez-Cuadrado L, Tracey N, Ma R, Qian B and Brunton VG: Mouse models of metastasis: Progress and prospects. Dis Model Mech 10: 1061-1074, 2017.
25. Estrella V, Chen T, Lloyd M, Wojtkowiak J, Cornnell HH, Ibrahim-Hashim A, Bailey K, Balagurunathan Y, Rothberg JM, Sloane BF, *et al*: Acidity generated by the tumor microenvironment drives local invasion. Cancer Res 73: 1524-1535, 2013.
26. Chen WJ, Ho CC, Chang YL, Chen HY, Lin CA, Ling TY, Yu SL, Yuan SS, Chen YJ, Lin CY, *et al*: Cancer-associated fibroblasts regulate the plasticity of lung cancer stemness via paracrine signalling. Nat Commun 5: 3472, 2014.
27. Peppicelli S, Bianchini F, Torre E and Calorini L: Contribution of acidic melanoma cells undergoing epithelial-to-mesenchymal transition to aggressiveness of non-acidic melanoma cells. Clin Exp Metastasis 31: 423-433, 2014.
28. Chen S, Zhou Y, Chen Y and Gu J: Fastp: An ultra-fast all-in-one FASTQ preprocessor. Bioinformatics 34: i884-i890, 2018.
29. Liao Y, Smyth GK and Shi W: FeatureCounts: An efficient general purpose program for assigning sequence reads to genomic features. Bioinformatics 30: 923-930, 2014.
30. Love MI, Huber W and Anders S: Moderated estimation of fold change and dispersion for RNA-seq data with DESeq2. Genome Biol 15: 550, 2014.
31. Robinson MD, McCarthy DJ and Smyth GK: edgeR: A bioconductor package for differential expression analysis of digital gene expression data. Bioinformatics 26: 139-140, 2010.
32. Bu D, Luo H, Huo P, Wang Z, Zhang S, He Z, Wu Y, Zhao L, Liu J, Guo J, *et al*: KOBAS-i: Intelligent prioritization and exploratory visualization of biological functions for gene enrichment analysis. Nucleic Acids Res 49 (W1): W317-W325, 2021.
33. Ruzzolini J, Peppicelli S, Andreucci E, Bianchini F, Margheri F, Laurenzana A, Fibbi G, Pimpinelli N and Calorini L: Everolimus selectively targets vemurafenib resistant $BRAF^{V600E}$ melanoma cells adapted to low pH. Cancer Lett 408: 43-54, 2017.
34. Su T, Huang S, Zhang Y, Guo Y, Zhang S, Guan J, Meng M, Liu L, Wang C, Yu D, *et al*: miR-7/TGF-β2 axis sustains acidic tumor microenvironment-induced lung cancer metastasis. Acta Pharm Sin B 12: 821-837, 2022.
35. Andreucci E, Peppicelli S, Ruzzolini J, Bianchini F, Biagioni A, Papucci L, Magnelli L, Mazzanti B, Stecca B and Calorini L: The acidic tumor microenvironment drives a stem-like phenotype in melanoma cells. J Mol Med (Berl) 98: 1431-1446, 2020.
36. Choodetwattana P, Proungvitaya S, Jearanaikoon P and Limpaiboon T: The upregulation of OCT4 in acidic extracellular pH is associated with gemcitabine resistance in cholangiocarcinoma cell lines. Asian Pac J Cancer Prev 20: 2745-2748, 2019.
37. Murlidhar V, Reddy RM, Fouladdel S, Zhao L, Ishikawa MK, Grabauskiene S, Zhang Z, Lin J, Chang AC, Carrott P, *et al*: Poor prognosis indicated by venous circulating tumor cell clusters in early-stage lung cancers. Cancer Res 77: 5194-5206, 2017.
38. Edgar R, Domrachev M and Lash AE: Gene expression omnibus: NCBI gene expression and hybridization array data repository. Nucleic Acids Res 30: 207-210, 2002.
39. Hynes RO: Integrins: Bidirectional, allosteric signaling machines. Cell 110: 673-687, 2002.
40. Cardones AR, Murakami T and Hwang ST: CXCR4 enhances adhesion of B16 tumor cells to endothelial cells in vitro and in vivo via beta(1) integrin. Cancer Res 63: 6751-6757, 2003.
41. Wagenblast E, Soto M, Gutiérrez-Ángel S, Hartl CA, Gable AL, Maceli AR, Erard N, Williams AM, Kim SY, Dickopf S, *et al*: A model of breast cancer heterogeneity reveals vascular mimicry as a driver of metastasis. Nature 520: 358-362, 2015.
42. Young SA, McCabe KE, Bartakova A, Delaney J, Pizzo DP, Newbury RO, Varner JA, Schlaepfer DD and Stupack DG: Integrin α4 enhances metastasis and may be associated with poor prognosis in MYCN-low neuroblastoma. PLoS One 10: e0120815, 2015.
43. Bulian P, Shanafelt TD, Fegan C, Zucchetto A, Cro L, Nückel H, Baldini L, Kurtova AV, Ferrajoli A, Burger JA, *et al*: CD49d is the strongest flow cytometry-based predictor of overall survival in chronic lymphocytic leukemia. J Clin Oncol 32: 897-904, 2014.
44. Pulkka OP, Mpindi JP, Tynninen O, Nilsson B, Kallioniemi O, Sihto H and Joensuu H: Clinical relevance of integrin alpha 4 in gastrointestinal stromal tumours. J Cell Mol Med 22: 2220-2230, 2018.
45. Marusyk A, Tabassum DP, Altrock PM, Almendro V, Michor F and Polyak K: Non-cell-autonomous driving of tumour growth supports sub-clonal heterogeneity. Nature 514: 54-58, 2014.
46. Michl J, Wang Y, Monterisi S, Blaszczak W, Beveridge R, Bridges EM, Koth J, Bodmer WF and Swietach P: CRISPR-Cas9 screen identifies oxidative phosphorylation as essential for cancer cell survival at low extracellular pH. Cell Rep 38: 110493, 2022.
47. Anemone A, Consolino L, Conti L, Irrera P, Hsu MY, Villano D, Dastrù W, Porporato PE, Cavallo F and Longo DL: Tumour acidosis evaluated in vivo by MRI-CEST pH imaging reveals breast cancer metastatic potential. Br J Cancer 124: 207-216, 2021.
48. Munoz R, Man S, Shaked Y, Lee CR, Wong J, Francia G and Kerbel RS: Highly efficacious nontoxic preclinical treatment for advanced metastatic breast cancer using combination oral UFT-cyclophosphamide metronomic chemotherapy. Cancer Res 66: 3386-3391, 2006.
49. Minn AJ, Gupta GP, Siegel PM, Bos PD, Shu W, Giri DD, Viale A, Olshen AB, Gerald WL and Massagué J: Genes that mediate breast cancer metastasis to lung. Nature 436: 518-524, 2005.
50. Guy CT, Webster MA, Schaller M, Parsons TJ, Cardiff RD and Muller WJ: Expression of the neu protooncogene in the mammary epithelium of transgenic mice induces metastatic disease. Proc Natl Acad Sci USA 89: 10578-10582, 1992.
51. Yu IF, Yu YH, Chen LY, Fan SK, Chou HYE and Yang JT: A portable microfluidic device for the rapid diagnosis of cancer metastatic potential which is programmable for temperature and CO2. Lab Chip 14: 3621 3628, 2014.
52. Pang X, He X, Qiu Z, Zhang H, Xie R, Liu Z, Gu Y, Zhao N, Xiang Q and Cui Y: Targeting integrin pathways: Mechanisms and advances in therapy. Signal Transduct Target Ther 8: 1, 2023.
53. Sabatier L, Chen D, Fagotto-Kaufmann C, Hubmacher D, McKee MD, Annis DS, Mosher DF and Reinhardt DP: Fibrillin assembly requires fibronectin. Mol Biol Cell 20: 846-858, 2009.
54. Qian F, Vaux DL and Weissman IL: Expression of the integrin alpha 4 beta 1 on melanoma cells can inhibit the invasive stage of metastasis formation. Cell 77: 335-347, 1994.
55. Schlesinger M and Bendas G: Contribution of very late antigen-4 (VLA-4) integrin to cancer progression and metastasis. Cancer Metastasis Rev 34: 575-591, 2015.
56. Xie J, Yang P, Lin HP, Li Y, Clementino M, Fenske W, Yang C, Wang C and Wang Z: Integrin α4 up-regulation activates the hedgehog pathway to promote arsenic and benzo[α]pyrene co-exposure-induced cancer stem cell-like property and tumorigenesis. Cancer Lett 493: 143-155, 2020.

57. Malfuson JV, Boutin L, Clay D, Thépenier C, Desterke C, Torossian F, Guerton B, Anginot A, de Revel T, Lataillade JJ and Le Bousse-Kerdilès MC: SP/drug efflux functionality of hematopoietic progenitors is controlled by mesenchymal niche through VLA-4/CD44 axis. Leukemia 28: 853-864, 2014.
58. Golebiewska A, Brons NHC, Bjerkvig R and Niclou SP: Critical appraisal of the side population assay in stem cell and cancer stem cell research. Cell Stem Cell 8: 136-147, 2011.
59. Wu C and Alman BA: Side population cells in human cancers. Cancer Lett 268: 1-9, 2008.
60. Maniotis AJ, Folberg R, Hess A, Seftor EA, Gardner LM, Pe'er J, Trent JM, Meltzer PS and Hendrix MJ: Vascular channel formation by human melanoma cells in vivo and in vitro: Vasculogenic mimicry. Am J Pathol 155: 739-752, 1999.
61. Upile T, Jerjes W, Radhi H, Al-Khawalde M, Kafas P, Nouraei S and Sudhoff H: Vascular mimicry in cultured head and neck tumour cell lines. Head Neck Oncol 3: 55, 2011.
62. Fu R, Du W, Ding Z, Wang Y, Li Y, Zhu J, Zeng Y, Zheng Y, Liu Z and Huang JA: HIF-1α promoted vasculogenic mimicry formation in lung adenocarcinoma through NRP1 upregulation in the hypoxic tumor microenvironment. Cell Death Dis 12: 394, 2021.
63. He X, You J, Ding H, Zhang Z, Cui L, Shen X, Bian X, Liu Y and Chen J: Vasculogenic mimicry, a negative indicator for progression free survival of lung adenocarcinoma irrespective of first line treatment and epithelial growth factor receptor mutation status. BMC Cancer 21: 132, 2021.
64. Williamson SC, Metcalf RL, Trapani F, Mohan S, Antonello J, Abbott B, Leong HS, Chester CP, Simms N, Polanski R, *et al*: Vasculogenic mimicry in small cell lung cancer. Nat Commun 7: 13322, 2016.
65. Baeten CIM, Hillen F, Pauwels P, de Bruine AP and Baeten CGMI: Prognostic role of vasculogenic mimicry in colorectal cancer. Dis Colon Rectum 52: 2028-2035, 2009.
66. Ruffini F, Graziani G, Levati L, Tentori L, D'Atri S and Lacal PM: Cilengitide downmodulates invasiveness and vasculogenic mimicry of neuropilin 1 expressing melanoma cells through the inhibition of αvβ5 integrin. Int J Cancer 136: E545-E558, 2015.
67. Vartanian A, Stepanova E, Grigorieva I, Solomko E, Belkin V, Baryshnikov A and Lichinitser M: Melanoma vasculogenic mimicry capillary-like structure formation depends on integrin and calcium signaling. Microcirculation 18: 390-399, 2011.